Unconventional strengthening of the bipartite entanglement of a mixed spin-(1/2,1) Heisenberg dimer achieved through Zeeman splitting

Hana Čenčariková [1,*] and Jozef Strečka [2]

[1]*Institute of Experimental Physics, Slovak Academy of Sciences, Watsonova 47, 040 01 Košice, Slovakia*

[2]*Department of Theoretical Physics and Astrophysics, Faculty of Science, P. J. Šafárik University, Park Angelinum 9, 040 01 Košice, Slovakia*

Bipartite quantum and thermal entanglement is quantified within pure and mixed states of a mixed spin-(1/2, 1) Heisenberg dimer with the help of negativity. It is shown that the negativity, which may serve as a measure of the bipartite entanglement at zero as well as nonzero temperatures, strongly depends on intrinsic parameters—for instance, exchange and uniaxial single-ion anisotropy—in addition to extrinsic parameters such as temperature and magnetic field. It turns out that a rising magnetic field unexpectedly reinforces the bipartite entanglement due to the Zeeman splitting of energy levels, which lifts the twofold degeneracy of the quantum ferrimagnetic ground state. The maximal bipartite entanglement is thus reached within a quantum ferrimagnetic phase at sufficiently low but nonzero magnetic fields under the assumption that the gyromagnetic g factors of the spin-1/2 and spin-1 magnetic ions are equal and the uniaxial single-ion anisotropy is half of the exchange constant. It is suggested that the heterodinuclear complex [Ni(dpt)(H$_2$O)Cu(pba)] $\cdot$ 2H$_2$O [pba = 1,3-propylenebis(oxamato) and dpt = bis-(3-aminopropyl)amine], which affords an experimental realization of the mixed spin-(1/2, 1) Heisenberg dimer, remains strongly entangled up to relatively high temperatures (about 115 K) and magnetic fields (about 140 T) that are comparable with the relevant exchange constant.

I. INTRODUCTION

Molecular magnetic materials [1–4] are among the prominent solid-state resources for quantum computation and quantum information processing [5], because they can be used to build extremely dense and efficient memory devices implementing Grover's algorithm [6]. Grover's search algorithm requires a superposition of "single-particle" quantum states, whereas spin states of a single magnetic molecule with a sufficiently long relaxation time provide an available platform for the molecule's technological implementation on the grounds of single-molecule magnets [7–9]. Some quantum algorithms, such as Shor's factoring algorithm [10], however, require both superposition and entanglement of "many-particle" quantum states, which naturally occur in many-particle quantum spin systems forming basic building blocks of molecular-based magnetic materials.

Many-particle quantum spin systems have been extensively investigated in the context of quantum information processing due to the possibility of creation and distribution of quantum entanglement between specific spin units acting as qubits [11] as well as the speed-up of quantum computation and communication [12]. It is noteworthy that entanglement measures such as negativity [13–15] or concurrence [16] can be related via certain witnesses to thermodynamic quantities [17,18], which additionally offer an intriguing possibility for experimental testing [19–26]. Some quantum protocols such as a quantum teleportation of information cannot be even realized without many-particle entangled states [27–30].

Bearing all this in mind, it appears worthwhile to investigate how a degree of entanglement in quantum spin systems is affected by extrinsic parameters such as temperature and external magnetic field. From the viewpoint of possible technological applications, it is especially important to find out whether a quantum entanglement emergent at absolute zero temperature may persists as a thermal entanglement at sufficiently high temperatures. The quantity concurrence has been widely used in order to capture the strength of the bipartite thermal entanglement in several spin-1/2 quantum systems: dimer [12,31,32], trimer [33,34], tetramer [34–36], chain [37,38], ladder [38–40], tube [41,42], tetrahedral chain [43,44], trimerized chain [45], diamond chain [46–51], pentagonal chain [52], and branched chain [53,54].

On the other hand, one may take advantage of the negativity [15] as a quantitative measure of the Peres-Horodecki criterion [13,14] in order to capture the bipartite thermal entanglement of quantum spin systems involving carriers with higher spin angular momentum, which, to date, have been much less comprehensively investigated in comparison with spin-1/2 quantum systems. Although the rising spin magnitude generally suppresses the strength of the quantum entanglement, it surprisingly turns out that the thermal entanglement of the mixed spin-(1/2, S) quantum systems survives up to a higher threshold temperature as the spin magnitude S increases [55,56]. A reasonable choice of constituent spins may accordingly ensure an optimization of the thermal entanglement, which would be concurrently sufficiently strong and resistant with respect to rising temperature.

*Corresponding author: hcencar@saske.sk

Owing to this fact, mixed spin-(1/2, 1) quantum systems may provide a prospective platform for reaching sufficiently strong and thermally resistant entanglement. Up to now, the concept of negativity has been adapted to measure the strength of the thermal entanglement of the mixed spin-(1/2, 1) Heisenberg chain [57–61], the mixed spin-(1/2, 1) Heisenberg dimer [62–66], the mixed spin-(1/2, 1) XY dimer [67,68], as well as the mixed spin-(1/2, 1) Ising-Heisenberg diamond chain [69]. The external magnetic field turns out to be another significant control parameter, which may eventually cause strengthening of the thermal entanglement [57,62–67]. In agreement with common expectations, the threshold temperature, above which the thermal entanglement vanishes, is not elevated by a uniform magnetic field [57], whereas it may be just slightly enhanced when applying a nonuniform magnetic field [63,64]. A more noticeable enhancement of the threshold temperature can be achieved, however, by implementing various types of the magnetic anisotropy such as the exchange anisotropy [59,62,64,67], the uniaxial single-ion anisotropy [60,61], or the Dzyaloshinskii-Moriya anisotropy [66].

In the present paper, we will examine the strength of the quantum and thermal entanglement within pure and mixed states of a mixed spin-(1/2, 1) Heisenberg dimer with the exchange and uniaxial single-ion anisotropies in presence of the nonuniform magnetic field, which takes into consideration different values of the gyromagnetic g factors of the spin-1/2 and spin-1 magnetic ions. The present theoretical study is motivated by the molecular-based compound [Ni(dpt)(H$_2$O)Cu(pba)] · 2H$_2$O [pba = 1,3-propylenebis(oxamato) and dpt = bis-(3-aminopropyl)amine] [70], which could be classified as a heterodinuclear complex of the exchange-coupled spin-1/2 Cu^{2+} and spin-1 Ni^{2+} magnetic ions, henceforth abbreviated as the CuNi compound. In this regard, the present paper provides a missing link between theoretical findings for the mixed spin-(1/2, 1) quantum Heisenberg dimer and its real-world representative afforded by the CuNi compound [70].

The organization of this paper is as follows. An exact calculation for the negativity of the mixed spin-(1/2, 1) Heisenberg dimer in a magnetic field is presented in Sec. II. The most interesting results for the quantum and thermal entanglement of the mixed spin-(1/2, 1) Heisenberg dimer will be presented in Sec. III as functions of the exchange anisotropy, the uniaxial single-ion anisotropy, and the magnetic field together with the relevant theoretical prediction for the CuNi complex. A brief summary of the most important scientific achievements is presented in Sec. IV along with future outlooks and perspectives.

II. MODEL AND METHOD

In the present paper, we will investigate in detail the quantum and thermal entanglement of the mixed spin-(1/2, 1) Heisenberg dimer defined by the Hamiltonian

$$\hat{\mathcal{H}} = J[\Delta(\hat{S}^x \hat{\mu}^x + \hat{S}^y \hat{\mu}^y) + \hat{S}^z \hat{\mu}^z] + D(\hat{\mu}^z)^2 - g_1 \mu_B B \hat{S}^z - g_2 \mu_B B \hat{\mu}^z, \quad (1)$$

where $\hat{S}^\alpha$ and $\hat{\mu}^\alpha$ ($\alpha = x, y, z$) denote spatial components of the spin-1/2 and spin-1 operators, respectively. The coupling constant J determines the Heisenberg exchange interaction between the spin-1/2 and spin-1 magnetic ions, the parameter Δ determines the XXZ exchange anisotropy in this exchange interaction, and the parameter D is a uniaxial single-ion anisotropy acting on the spin-1 magnetic ions only. Finally, the parameter B denotes a static external magnetic field, μ_B is the Bohr magneton, while g_1 and g_2 are Landé g factors of the spin-1/2 and spin-1 magnetic ions, respectively.

A matrix representation of the Hamiltonian (1) in the standard basis formed by the eigenvectors $|\varphi_i\rangle \in \{|\frac{1}{2}, 1\rangle, |\frac{1}{2}, 0\rangle, |\frac{1}{2}, -1\rangle, |-\frac{1}{2}, 1\rangle, |-\frac{1}{2}, 0\rangle, |-\frac{1}{2}, -1\rangle\}$ of z-components of the constituting spin-1/2 and spin-1 entities reads as follows:

$$\langle \varphi_j | \hat{\mathcal{H}} | \varphi_i \rangle = \begin{pmatrix} H_{11} & 0 & 0 & 0 & 0 & 0 \\ 0 & H_{22} & 0 & H_{24} & 0 & 0 \\ 0 & 0 & H_{33} & 0 & H_{35} & 0 \\ 0 & H_{42} & 0 & H_{44} & 0 & 0 \\ 0 & 0 & H_{53} & 0 & H_{55} & 0 \\ 0 & 0 & 0 & 0 & 0 & H_{66} \end{pmatrix}, \quad (2)$$

whereas six diagonal elements are defined by

$$H_{11} = \frac{1}{2}[J + 2D - (h_1 + 2h_2)],$$

$$H_{22} = -\frac{h_1}{2},$$

$$H_{33} = -\frac{1}{2}[J - 2D + (h_1 - 2h_2)],$$

$$H_{44} = -\frac{1}{2}[J - 2D - (h_1 - 2h_2)], \quad (3)$$

$$H_{55} = \frac{h_1}{2},$$

$$H_{66} = \frac{1}{2}[J + 2D + (h_1 + 2h_2)],$$

and four off-diagonal elements are equal to

$$H_{24} = H_{42} = H_{35} = H_{53} = \frac{J\Delta}{\sqrt{2}}. \quad (4)$$

For abbreviation purposes, we have introduced above two new parameters, $h_1 = g_1 \mu_B B$ and $h_2 = g_2 \mu_B B$, related to "local" Zeeman terms (magnetic fields) acting on the spin-1/2 and spin-1 magnetic particles, which may be different due to difference of the gyromagnetic g factors $g_1 \neq g_2$. A relatively simple (sparse) structure of the Hamiltonian matrix (2) allows us to obtain a complete set of eigenvalues by an exact analytical diagonalization,

$$E_{1,2} = \frac{1}{2}[J + 2D \mp (h_1 + 2h_2)], \quad (5)$$

$$E_{3,4} = -\frac{1}{4}(J - 2D + 2h_2) \mp \frac{1}{4}\sqrt{[J - 2D - 2(h_1 - h_2)]^2 + 8(J\Delta)^2}, \quad (6)$$

$$E_{5,6} = -\frac{1}{4}(J - 2D - 2h_2) \mp \frac{1}{4}\sqrt{[J - 2D + 2(h_1 - h_2)]^2 + 8(J\Delta)^2}, \quad (7)$$

whereas the corresponding eigenvectors read

$$|\psi_1\rangle = \left|\tfrac{1}{2}, 1\right\rangle, \tag{8}$$

$$|\psi_2\rangle = \left|-\tfrac{1}{2}, -1\right\rangle, \tag{9}$$

$$|\psi_{3,4}\rangle = c_1^{\mp}\left|\tfrac{1}{2}, 0\right\rangle \mp c_1^{\pm}\left|-\tfrac{1}{2}, 1\right\rangle, \tag{10}$$

$$|\psi_{5,6}\rangle = c_2^{\pm}\left|\tfrac{1}{2}, -1\right\rangle \mp c_2^{\mp}\left|-\tfrac{1}{2}, 0\right\rangle. \tag{11}$$

The last four eigenvectors (10) and (11) are defined through the probability amplitudes

$$c_1^{\pm} = \frac{1}{\sqrt{2}}\sqrt{1 \pm \frac{J - 2D - 2(h_1 - h_2)}{\sqrt{[J - 2D - 2(h_1 - h_2)]^2 + 8(J\Delta)^2}}}, \tag{12}$$

$$c_2^{\pm} = \frac{1}{\sqrt{2}}\sqrt{1 \pm \frac{J - 2D + 2(h_1 - h_2)}{\sqrt{[J - 2D + 2(h_1 - h_2)]^2 + 8(J\Delta)^2}}}.$$

To explore a degree of quantum and thermal entanglement in pure and mixed states of the mixed spin-$(1/2, 1)$ Heisenberg dimer, one may employ the quantity negativity [15] serving as a measure of the pairwise entanglement according to Peres-Horodecki separability criterion [13,14]

$$\mathcal{N} = \sum_{i=1}^{6} \frac{|\lambda_i| - \lambda_i}{2}, \tag{13}$$

which is defined through eigenvalues λ_i of a partially transposed density matrix $\rho^{T_{1/2}}$ derived from the overall density matrix ρ upon a partial transposition $T_{1/2}$ with respect to one subsystem. In this particular case $T_{1/2}$ denotes a partial transposition with respect to states of the spin-$1/2$ magnetic ion. According to the Peres-Horodecki separability criterion [13,14], invented for partially transposed density matrices, the negativity becomes zero ($\mathcal{N} = 0$) for separable (factorizable) states, while it becomes nonzero ($\mathcal{N} \neq 0$) for entangled (nonseparable) states. Consequently, the necessary and sufficient prerequisite for detecting a quantum or thermal entanglement within pure or mixed states of the mixed spin-$(1/2, 1)$ Heisenberg dimer is at least one negative eigenvalue λ_i of the partially transposed density matrix $\rho^{T_{1/2}}$.

The density operator $\hat{\rho}$ of the mixed spin-$(1/2, 1)$ Heisenberg dimer can be easily calculated from the eigenvalues (5)–(7) and the respective eigenvectors (8)–(11) according to the formula

$$\hat{\rho} = \frac{1}{Z}\sum_{i=1}^{6} \exp(-\beta E_i)|\psi_i\rangle\langle\psi_i|, \tag{14}$$

which is expressed in terms of the partition function $Z = \sum_{i=1}^{6} \exp(-\beta E_i)$, giving the following explicit form:

$$Z = 2\left\{ e^{-\frac{\beta}{2}(J+2D)}\cosh\left[\frac{\beta}{2}(h_1 + 2h_2)\right] + e^{\frac{\beta}{4}(J-2D)} \right.$$
$$\times \left[e^{\frac{\beta h_2}{2}}\cosh\left(\frac{\beta}{4}\sqrt{[J - 2D - 2(h_1 - h_2)]^2 + 8(J\Delta)^2}\right) \right.$$
$$\left.\left. + e^{-\frac{\beta h_2}{2}}\cosh\left(\frac{\beta}{4}\sqrt{[J-2D+2(h_1-h_2)]^2+8(J\Delta)^2}\right) \right]\right\}. \tag{15}$$

Of course, the density matrix corresponding to the density operator (14) has a matrix structure similar to the Hamiltonian matrix (2),

$$\rho = \begin{pmatrix} \rho_{11} & 0 & 0 & 0 & 0 & 0 \\ 0 & \rho_{22} & 0 & \rho_{24} & 0 & 0 \\ 0 & 0 & \rho_{33} & 0 & \rho_{35} & 0 \\ 0 & \rho_{42} & 0 & \rho_{44} & 0 & 0 \\ 0 & 0 & \rho_{53} & 0 & \rho_{55} & 0 \\ 0 & 0 & 0 & 0 & 0 & \rho_{66} \end{pmatrix}, \tag{16}$$

whereas individual elements ρ_{ij} of the density matrix are, for the sake of brevity, explicitly given in Appendix A. A partial transposition $T_{1/2}$ with respect to states of the spin-$1/2$ magnetic ion gives the partially transposed density matrix

$$\rho^{T_{1/2}} = \begin{pmatrix} \rho_{11} & 0 & 0 & 0 & \rho_{24} & 0 \\ 0 & \rho_{22} & 0 & 0 & 0 & \rho_{35} \\ 0 & 0 & \rho_{33} & 0 & 0 & 0 \\ 0 & 0 & 0 & \rho_{44} & 0 & 0 \\ \rho_{24} & 0 & 0 & 0 & \rho_{55} & 0 \\ 0 & \rho_{35} & 0 & 0 & 0 & \rho_{66} \end{pmatrix}, \tag{17}$$

which has the following spectrum of eigenvalues:

$$\lambda_1 = \rho_{33}, \tag{18}$$

$$\lambda_2 = \rho_{44}, \tag{19}$$

$$\lambda_{3,4} = \frac{\rho_{22} + \rho_{66}}{2} \pm \frac{1}{2}\sqrt{(\rho_{22} - \rho_{66})^2 + 4\rho_{35}^2}, \tag{20}$$

$$\lambda_{5,6} = \frac{\rho_{11} + \rho_{55}}{2} \pm \frac{1}{2}\sqrt{(\rho_{55} - \rho_{11})^2 + 4\rho_{24}^2}. \tag{21}$$

It is quite clear that the eigenvalues λ_4 and λ_6 with negative sign before a square root may become, under certain conditions, negative, which according to the definition (13) is a necessary prerequisite of nonzero negativity (bipartite entanglement). In the following part we will investigate in detail manifestation of quantum and thermal entanglement of the mixed spin-$(1/2, 1)$ Heisenberg dimer depending on temperature, magnetic field, and magnetic anisotropy.

III. RESULTS AND DISCUSSION

It is worthwhile to recall that suitable experimental realizations of the mixed spin-$(1/2, 1)$ Heisenberg dimer are offered by heterobimetallic complexes such as the CuNi compound [70], which is composed of exchange coupled spin-$1/2$ Cu^{2+} and spin-1 Ni^{2+} magnetic ions. Note furthermore that transition-metal ions, for instance Cu^{2+} and Ni^{2+}, usually have gyromagnetic g factors quite close to the spin-only value $g = 2$ due to an almost full quenching of their orbital momentum [1–3]. In this regard, we will consider hereafter three different combinations of Landé g factors: (i) $g_1 = g_2 = 2.0$, (ii) $g_1 = 2.2$, $g_2 = 2.0$, and (iii) $g_1 = 2.0$, $g_2 = 2.2$. The first case bears a close relation to the ideal case with equal gyromagnetic factors with the spin-only value $g = 2$, while in the second and third cases the gyromagnetic factor of the spin-$1/2$ magnetic ion Cu^{2+} slightly exceeds the one of the spin-1 magnetic ion Ni^{2+} or vice versa. For simplicity, the size of the antiferromagnetic exchange interaction $J > 0$ may serve as an energy unit when defining a set of dimensionless

quantities measuring a relative strength of the uniaxial single-ion anisotropy D/J, magnetic field $\mu_B B/J$, and temperature $k_B T/J$.

A. Quantum entanglement

First, we pay attention to a comprehensive analysis of a bipartite quantum entanglement of the mixed spin-$(1/2, 1)$ Heisenberg dimer at zero temperature and magnetic field depending on two intrinsic model parameters, Δ and D/J, determining the exchange and uniaxial single-ion anisotropies, respectively. The zero-field ground state of the mixed spin-$(1/2, 1)$ Heisenberg dimer could be classified as a twofold degenerate quantum ferrimagnetic state given by the eigenvectors

$$|\text{QFI}_{\pm}\rangle = \begin{cases} c_0^+ | -1/2, 1\rangle - c_0^- |1/2, 0\rangle, \\ c_0^+ |1/2, -1\rangle - c_0^- | -1/2, 0\rangle, \end{cases} \quad (22)$$

where the probability amplitudes $c_0^{\pm}$ unambiguously determine the relevant quantum superposition of the microstates $|\mp 1/2, 1\rangle$ and $|\pm 1/2, 0\rangle$ are given by

$$c_0^{\pm} = \frac{1}{\sqrt{2}} \left(\sqrt{1 \pm \frac{1 - 2\frac{D}{J}}{\sqrt{\left(1 - 2\frac{D}{J}\right)^2 + 8\Delta^2}}} \right). \quad (23)$$

Using the respective density operator $\hat{\rho} = (|\text{QFI}_+\rangle\langle\text{QFI}_+| + |\text{QFI}_-\rangle\langle\text{QFI}_-|)/2$, one gets the following zero-temperature value of the negativity that characterizes the bipartite entanglement within a twofold degenerate quantum ferrimagnetic ground state (22) at zero magnetic field:

$$\mathcal{N} = \frac{\sqrt{\left(1 - 2\frac{D}{J}\right)^2 + 8\Delta^2} - \left(1 - 2\frac{D}{J}\right)}{4\sqrt{\left(1 - 2\frac{D}{J}\right)^2 + 8\Delta^2}}$$

$$\times \left[\sqrt{\frac{5\sqrt{\left(1 - 2\frac{D}{J}\right)^2 + 8\Delta^2} + 3\left(1 - 2\frac{D}{J}\right)}{\sqrt{\left(1 - 2\frac{D}{J}\right)^2 + 8\Delta^2} - \left(1 - 2\frac{D}{J}\right)}} - 1 \right]. \quad (24)$$

It appears worthwhile to examine in somewhat more detail a degree of the bipartite quantum entanglement of the mixed spin-$(1/2, 1)$ Heisenberg dimer in zero magnetic field depending on a relative strength of the exchange and uniaxial single-ion anisotropy. To this end, the negativity is plotted in Fig. 1 against the uniaxial single-ion anisotropy for three representative values of the exchange anisotropy, namely, the fully isotropic case ($\Delta = 1.0$) and the particular cases with easy-axis ($\Delta = 0.5$) and easy-plane ($\Delta = 2.0$) exchange anisotropies. It is evident from Fig. 1 that the negativity shows a relatively broad maximum at $\mathcal{N} = 1/3$, whose position depends on a specific choice of the exchange anisotropy. For instance, the mixed spin-$(1/2, 1)$ Heisenberg dimer with a perfectly isotropic exchange interaction $\Delta = 1$ exhibits the strongest bipartite quantum entanglement under the assumption that the uniaxial single-ion anisotropy is also absent $D/J = 0$, i.e., it does not possess any form of the magnetic anisotropy. On the other hand, the easy-axis (easy-plane) exchange anisotropy $\Delta < 1$ ($\Delta > 1$) shifts the local maximum of the negativity towards the uniaxial single-ion anisotropy with an easy-plane (easy-axis) character $D/J > 0$ ($D/J < 0$)
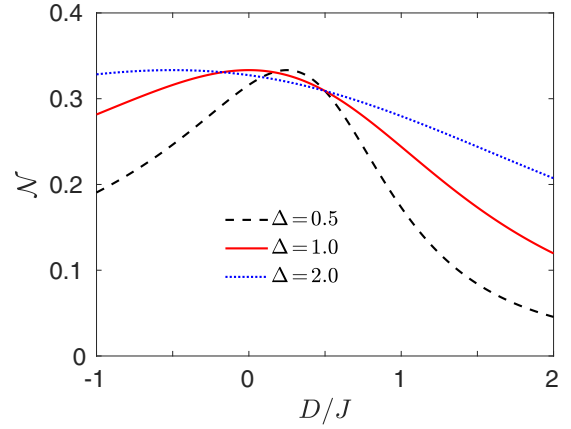

FIG. 1. The negativity as a function of the uniaxial single-ion anisotropy D/J for three different values of the exchange anisotropy, $\Delta = 0.5$, 1.0, and 2.0, at zero magnetic field.

competing with the exchange anisotropy. It is also worthwhile to note that a relative strength of the bipartite quantum entanglement becomes, according to Eq. (24), independent of the exchange anisotropy for the particular value of the uniaxial single-ion anisotropy $D/J = 1/2$, for which the negativity acquires half of the golden-ratio conjugate $\mathcal{N} = (\sqrt{5} - 1)/4 \approx 0.309$ regardless of the anisotropy parameter Δ (see the crossing point in Fig. 1).

Next, let us investigate in detail a strength of the bipartite quantum entanglement of the mixed spin-$(1/2, 1)$ Heisenberg dimer at zero temperature for three considered settings of Landé g factors in the presence of an external magnetic field. For this purpose, we have plotted first in Fig. 2 the ground-state phase diagrams of the mixed spin-$(1/2, 1)$ Heisenberg dimer in the D/J-$\mu_B B/J$ plane for three different values of the exchange anisotropy, $\Delta = 0.5$, 1.0, and 2.0. Of course, a sufficiently strong magnetic field gives rise to the classical ferromagnetic state $|\text{FM}\rangle = |1/2, 1\rangle$, which is naturally
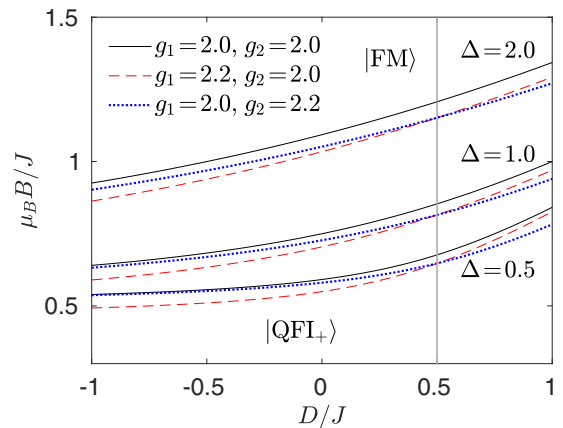

FIG. 2. The ground-state phase diagram in the D/J-$\mu_B B/J$ plane for three selected values of the exchange anisotropy, $\Delta = 0.5$, 1.0, 2.0, and three different sets of the Landé g factors indicated in the legend. A thin vertical line at $D/J = 1/2$ determines a special value of the uniaxial single-ion anisotropy, at which the respective transition field becomes independent of the difference $|g_1 - g_2|$.

without any quantum entanglement as evidenced by a zero value of the negativity, $\mathcal{N} = 0$. On the other hand, the twofold degeneracy of the quantum ferrimagnetic ground state (22) is lifted by the external magnetic field due to the Zeeman splitting of energy levels, which stabilizes at sufficiently low but nonzero magnetic fields the unique quantum ferrimagnetic ground state:

$$|\text{QFI}_+\rangle = c_1^+ |-1/2, 1\rangle - c_1^- |1/2, 0\rangle. \quad (25)$$

The unique quantum ferrimagnetic ground state (25) is characterized by a quantum superposition of the microstates $|-1/2, 1\rangle$ and $|1/2, 0\rangle$ unambiguously given by the following probability amplitudes:

$$c_1^\pm = \frac{1}{\sqrt{2}} \sqrt{1 \pm \frac{1 - 2\frac{D}{J} - 2\frac{\mu_B B}{J}(g_1 - g_2)}{\sqrt{\left[1 - 2\frac{D}{J} - 2\frac{\mu_B B}{J}(g_1 - g_2)\right]^2 + 8\Delta^2}}}. \quad (26)$$

The respective zero-temperature asymptotic value of the negativity for the nondegenerate quantum ferrimagnetic ground state $|\text{QFI}_+\rangle$ given by Eq. (25) can be acquired by making use of the density operator $\hat{\rho} = |\text{QFI}_+\rangle\langle\text{QFI}_+|$:

$$\mathcal{N} = \frac{\sqrt{2}\Delta}{\sqrt{\left[1 - 2\frac{D}{J} - 2(g_1 - g_2)\frac{\mu_B B}{J}\right]^2 + 8\Delta^2}}. \quad (27)$$

At fixed values of the model parameters, the specific value of the negativity (27) pertinent to the nondegenerate quantum ferrimagnetic ground state $|\text{QFI}_+\rangle$ is surprisingly much greater at nonzero magnetic fields than the zero-field value (24) inherent to the twofold degenerate quantum ferrimagnetic phase $|\text{QFI}_\pm\rangle$ forming the respective ground state in the zero-field limit. It could be thus concluded that the Zeeman splitting of energy levels due to the external magnetic field leads to an unexpected sudden rise of the bipartite quantum entanglement of the mixed spin-(1/2, 1) Heisenberg dimer, which is in contrast with the naive expectation that the magnetic field suppresses the quantum entanglement. Moreover, it will be shown herein that the sudden rise of the bipartite entanglement due to rising magnetic field at absolute zero temperature is also preserved at sufficiently small but nonzero temperatures, which makes this feature especially interesting with regard to possible experimental testing (see Sec. III B).

The phase boundary between the classical ferromagnetic $|\text{FM}\rangle$ and quantum ferrimagnetic $|\text{QFI}_+\rangle$ ground states follows from the formula

$$\frac{\mu_B B}{J} = \frac{1}{4g_1 g_2}\left[g_1 + 2g_2 + 2g_1\frac{D}{J}\right.$$
$$\left. + \sqrt{\left(g_1 - 2g_2 + 2g_1\frac{D}{J}\right)^2 + 8g_1 g_2 \Delta^2}\right], \quad (28)$$

which depends on a mutual interplay of the exchange anisotropy Δ, the uniaxial single-ion anisotropy D/J, as well as the g factors g_1 and g_2. In general, an increase of both anisotropy parameters D/J and Δ stabilizes the quantum ferrimagnetic ground state $|\text{QFI}_+\rangle$, while the rising magnetic field $\mu_B B/J$ contrarily stabilizes the classical ferromagnetic ground state $|\text{FM}\rangle$. A shift of the gyromagnetic g factors from their spin-only value also promotes existence of the classical ferromagnetic ground state $|\text{FM}\rangle$ at the expense of the quantum ferrimagnetic ground state $|\text{QFI}_+\rangle$; however, this impact is rather insignificant for reasonable values of gyromagnetic ratios $g_{1,2} \gtrsim 2$. In addition, it can be clearly seen from Fig. 2 that the ground-state phase boundaries for two particular cases with unequal g factors cross each other at the special value of the uniaxial single-ion anisotropy $D/J = 1/2$ when assuming the same value of the exchange anisotropy Δ, because the transition field is, in accordance with Eq. (28), independent of the difference of the gyromagnetic g factors $|g_1 - g_2|$. Zero-temperature density plots of the negativity $\mathcal{N}$, which quantifies a degree of the bipartite quantum entanglement within the mixed spin-(1/2, 1) Heisenberg dimer, are depicted in Fig. 3 in the D/J-$\mu_B B/J$ plane for three different sets of Landé g factors and two representative values of the exchange anisotropy, $\Delta = 0.5$ and 1.0. In agreement with the formula (27), the negativity $\mathcal{N}$ becomes within the quantum ferrimagnetic phase (25) fully independent of a relative strength of the magnetic field $\mu_B B/J$ under the assumption that the gyromagnetic factors are set equal to each other, $g_1 = g_2$ (see left panels in Fig. 3). Even under the specific constraint $g_1 = g_2$, the anisotropic parameters D/J and Δ still significantly influence the strength of the bipartite quantum entanglement; for instance, the negativity $\mathcal{N}$ is in general reinforced upon increasing the parameter Δ. As far as the influence of the uniaxial single-ion anisotropy is concerned, the maximal value of the negativity $\mathcal{N} = 0.5$ is notably reached for the particular case with $D/J = 1/2$ (see the vertical white lines in the left panels of Fig. 3), whereas the negativity gradually diminishes as one moves further apart from this specific case to the highly anisotropic cases $D/J \to \pm\infty$.

A situation for the more general case with different gyromagnetic g factors, $g_1 \neq g_2$, is much more involved. The contours with extremal values of the negativity in the middle and right panels of Fig. 3, along which the negativity achieves the maximal value $\mathcal{N} = 0.5$, are apparently not vertical, but they deflect from a vertical direction by the specific angle α, which is proportional to the difference of Landé g factors, $\alpha = \arctan(g_2 - g_1)$. It is noteworthy that the same trend is preserved also for contours, which do not correspond to the extremal value of the negativity. Owing to the inclination of the contours from the magnetic-field axis, the negativity may thus gradually increase or decrease upon variation of the magnetic field. Moreover, the increasing magnetic field may eventually initially enhance and subsequently reduce the negativity in the parameter region circumscribed by the specific values of the uniaxial single-ion anisotropy $D/J = 1/2$ and $D/J = [2g_2 - g_1 - \sqrt{2}\Delta(g_1 - g_2)]/2g_1$ before the field-driven transition between the quantum ferrimagnetic and classical ferromagnetic phases finally takes place.
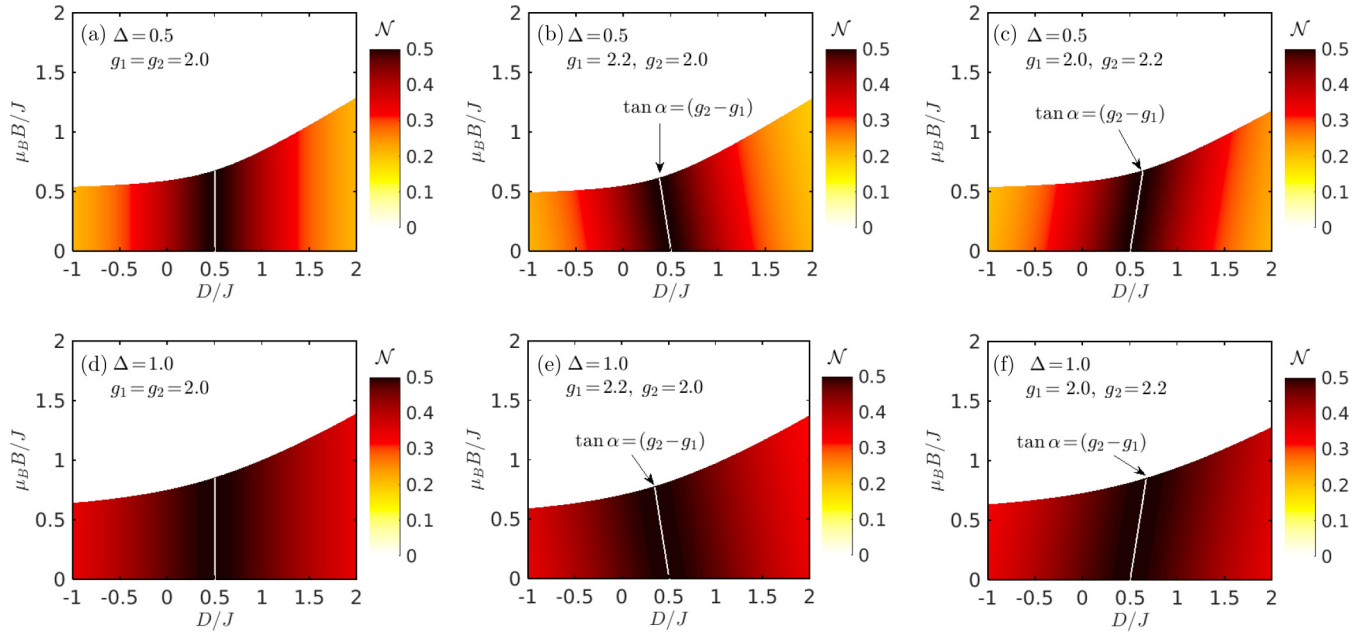
FIG. 3. Zero-temperature density plots of the negativity $\mathcal{N}$ in the D/J-$\mu_B B/J$ plane for three different sets of Landé g factors specified in the panels and two selected values of the exchange anisotropy, $\Delta = 0.5$ (upper panels) and 1.0 (lower panels). A thin (white) line starting from $D/J = 1/2$ determines the contour line for the maximal value of the negativity, $\mathcal{N} = 0.5$.

B. Thermal entanglement

Now, let us investigate in detail how the bipartite entanglement of the mixed spin-(1/2, 1) Heisenberg dimer is resistant with respect to thermal fluctuations. The magnetic-field dependence of the negativity is shown in Fig. 4 for the specific case with $g_1 = g_2$ and $\Delta = 1.0$ at a few selected values of temperature and two different values of the uniaxial single-ion anisotropy, which are equally distant from the particular value $D/J = 1/2$ bringing about the strongest quantum entanglement $\mathcal{N} = 0.5$. It is evident from Fig. 4 that the thermal entanglement is surprisingly enhanced upon increasing the magnetic field, as evidenced by a significant round maximum of the negativity observable for sufficiently low temperatures regardless of whether the uniaxial single-ion anisotropy is of easy-axis [Fig. 4(a)] or easy-plane [Fig. 4(b)] type. The unconventional enhancement of the thermal entanglement due to the magnetic field can be again related to Zeeman's splitting of two energy levels, which form the twofold degenerate quantum ferrimagnetic ground state (22) in the zero-field limit. As a matter of fact, the negativity converges at sufficiently low temperatures to the specific value (27), which coincides with a degree of the quantum entanglement of the nondegenerate quantum ferrimagnetic ground state (25).

To examine the influence of the uniaxial single-ion anisotropy on the thermal entanglement, a few density plots of the negativity $\mathcal{N}$ are displayed in Fig. 5 in the temperature-field plane by assuming the equal g factors $g_1 = g_2 = 2.0$, the fixed value of the exchange anisotropy $\Delta = 1.0$, and four different values of the uniaxial single-ion anisotropy D/J. It follows from the displayed density plots that a strong enough thermal entanglement can be detected only if temperature and magnetic field are simultaneously smaller than the exchange constant, i.e., $k_B T/J \lesssim 1$ and $\mu_B B/J \lesssim 1$. Moreover,
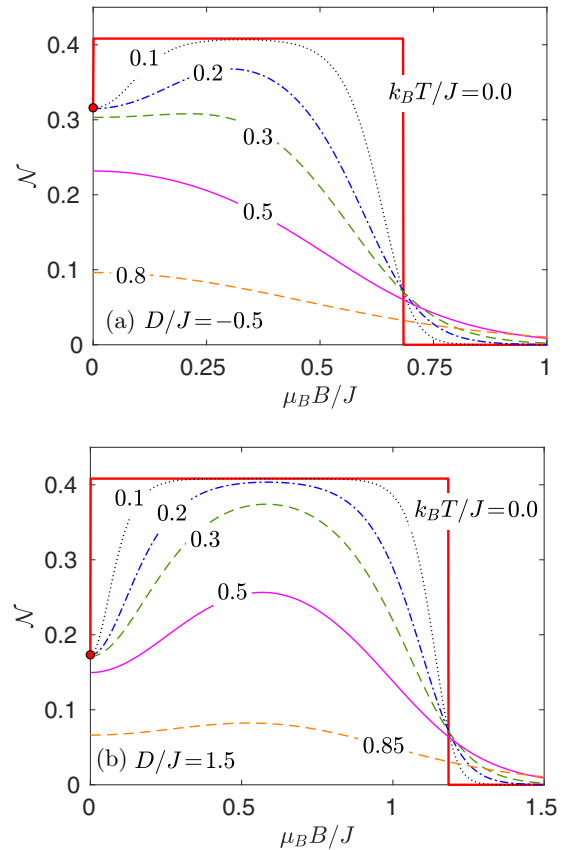

FIG. 4. The negativity as a function of the magnetic field for $\Delta = 1.0$, $g_1 = g_2 = 2.0$ by considering a few different values of temperature and two selected values of the uniaxial single-ion anisotropy: (a) $D/J = -0.5$, (b) $D/J = 1.5$. Red circled points determine a zero-field limit of the negativity for the absolute zero temperature.
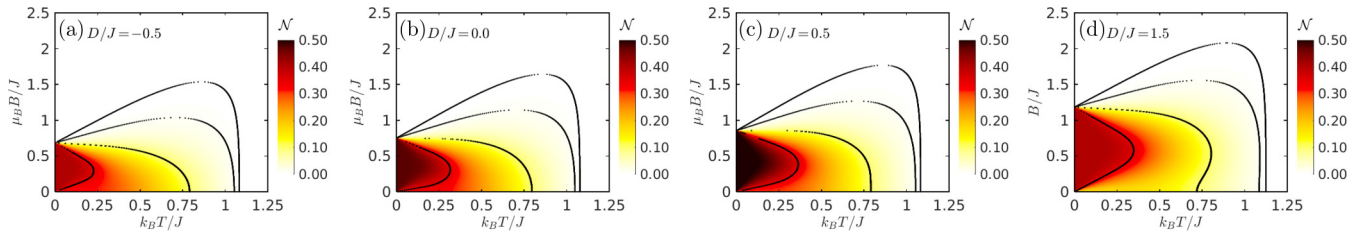
FIG. 5. Density plots of the negativity $\mathcal{N}$ in the $k_B T/J$-$\mu_B B/J$ plane for $\Delta = 1.0$, $g_1 = g_2 = 2.0$, and four different values of the uniaxial single-ion anisotropy, $D/J = -0.5$, 0.0, 0.5, and 1.5. The black contour lines correspond to the specific values of $\mathcal{N} = 0.35$, 0.1, 0.01, and 0.001 (from left to right).

the strongest thermal entanglement can be detected when the uniaxial single-ion anisotropy is sufficiently close to the specific value $D/J = 1/2$, which gives rise to the highest possible value of the negativity $\mathcal{N} = 0.5$ in the zero-temperature limit. It is also worth noticing that the thermal entanglement exhibits an intriguing reentrant behavior when the external magnetic field is selected slightly above the saturation value. Under this condition, the negativity is initially zero at low enough temperatures, then it starts to develop above a lower threshold temperature until it reaches a local maximum, and, finally, the negativity gradually diminishes upon further increase of temperature until it completely disappears above an upper threshold temperature. A black contour line shown in Fig. 5 for the smallest value of the negativity indeed corroborates a temperature-driven reentrance of the thermal entanglement. In contrast to general expectations, this result means that the relatively small thermal entanglement can be counterintuitively generated above the classical ferromagnetic ground state upon increasing the temperature.

Next, our particular attention will be focused on how difference between the Landé g factors may influence the thermal entanglement. To this end, the negativity $\mathcal{N}$ is plotted in Fig. 6 against the magnetic field for both types of differences of Landé g factors, $g_1 > g_2$ and $g_1 < g_2$, respectively, the fixed value of the exchange anisotropy $\Delta = 1.0$, a few selected values of temperature $k_B T/J$, and four different values of the uniaxial single-ion anisotropy D/J. Generally, the quantitative differences between the negativities for both considered settings of the gyromagnetic g factors are very subtle, mainly because of their small relative difference. It should be nevertheless pointed out that the negativity tends to the same asymptotic values in the zero-field limit as well as at high magnetic fields, while the most pronounced differences can be thus detected at moderate magnetic fields. It also follows from Fig. 6 that the zero-temperature asymptotic limit of the negativity shows in the low-field regime a quasilinear increase (decrease) for $g_1 > g_2$ under the assumption that $D/J < 1/2$ ($D/J > 1/2$), while the opposite trend applies for the other particular case with $g_1 < g_2$. Most importantly, the negativity for $g_1 < g_2$ mostly exceeds the one for $g_1 > g_2$ even though the reverse statement may hold in a zero- and low-temperature limit.

To provide a deeper insight, density plots of the negativity are depicted in Fig. 7 for the fixed value of the exchange anisotropy $\Delta = 1.0$, four different values of the uniaxial single-ion anisotropy D/J, and two different sets of Landé g factors, $g_1 > g_2$ and $g_1 < g_2$, respectively. In agreement with general expectations, the negativity mostly decreases upon increasing of temperature or magnetic field. The only

exceptions to this rule apply to magnetic fields slightly exceeding the saturation field when the thermal entanglement is enhanced upon increasing temperature, as well as to low enough temperatures when the increasing magnetic field gives rise to an enhancement of the thermal entanglement. It could be thus concluded that the negativity shows qualitatively the same generic features for both settings of the g factors, as discussed previously for the particular case $g_1 = g_2$. The marked difference in the respective density plots occurs just at relatively high temperatures $k_B T/J \gtrsim 1$ and magnetic fields $\mu_B B/J \gtrsim 1.5$, where a kink in contour lines of the negativity may be observed. Note furthermore that this nontrivial feature appears at very small values of the negativity $\mathcal{N} \lesssim 0.001$ just for $D/J < 1/2$ under the assumption that $g_1 > g_2$ [see Figs. 7(a)–7(c)], while the same anomaly of the negativity can be detected for $D/J > 1/2$ only if $g_1 < g_2$ [see Fig. 7(h)]. However, it is questionable if such a small value of the negativity can be experimentally detected. Last but not least, the contour plots shown in Figs. 7(d) and 7(h) convincingly show that the negativity may be reinforced upon increasing the magnetic field also at relatively high temperatures (e.g., $k_B T/J \lesssim 1$ for $D/J = 1.5$) whenever a sufficiently strong easy-plane single-ion anisotropy is considered.

C. Thermal entanglement in the CuNi complex

In this part we will put forward a theoretical prediction for a degree of quantum and thermal entanglement of the heterodinuclear complex CuNi [70], which affords an appropriate experimental realization of the mixed spin-(1/2, 1) Heisenberg dimer. It has been verified in Ref. [70] that the magnetic properties of the CuNi complex can be faithfully reproduced by the mixed spin-(1/2, 1) Heisenberg dimer with the relatively strong isotropic exchange constant $J/k_B = 141$ K and the gyromagnetic g factors $g_1 = 2.20$ for Cu^{2+} and $g_2 = 2.29$ for Ni^{2+} magnetic ions, respectively, while any clear signatures of the exchange ($\Delta = 1$) or uniaxial single-ion ($D/k_B = 0$) anisotropy have not been found [70]. In the following we will therefore adapt this set of the model parameters in order to make the relevant theoretical prediction for the bipartite entanglement of the CuNi dimeric compound.

The negativity of the mixed spin-(1/2, 1) Heisenberg dimer with the isotropic exchange constant $J/k_B = 141$ K and the gyromagnetic g factors $g_1 = 2.20$ and $g_2 = 2.29$ is plotted in Fig. 8 as a function of temperature for a few selected values of the magnetic field and as a function of the magnetic field for a few selected temperatures. Temperature variations of the negativity displayed in Fig. 8(a) exhibit mostly a mono-
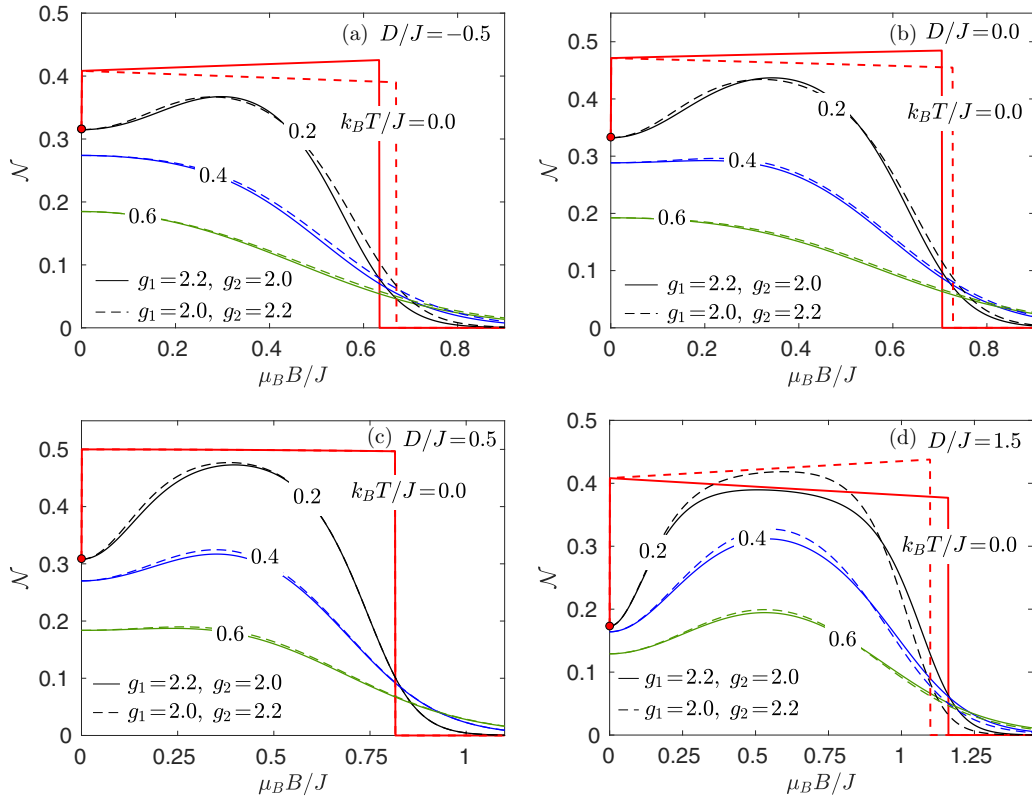
FIG. 6. The negativity as a function of the magnetic field for the fixed value of the exchange anisotropy $\Delta = 1.0$, a few different values of temperature, four selected vales of the uniaxial single-ion anisotropy $D/J = -0.5, 0.0, 0.5, 1.5$ and two different combinations of the gyromagnetic factors with equal difference $|g_1 - g_2| = 0.2$.

tonic decline with increasing temperature. At zero magnetic field the negativity monotonically decreases from the initial value $\mathcal{N} = 1/3$ until it completely vanishes at the threshold temperature $k_B T_t/J \approx 150$ K. At nonzero magnetic fields the negativity markedly starts from the local maximum $\mathcal{N} \approx 0.47$ which is relatively close to the highest possible value

$\mathcal{N} = 1/2$ for the mixed spin-$(1/2, 1)$ system, whereas the threshold temperature turns out to be independent of the magnetic field. An outstanding nonmonotonic thermal dependence of the negativity can be found only if the magnetic field surpasses the saturation value. Under this condition, the negativity become nonzero just at a lower threshold temperature,
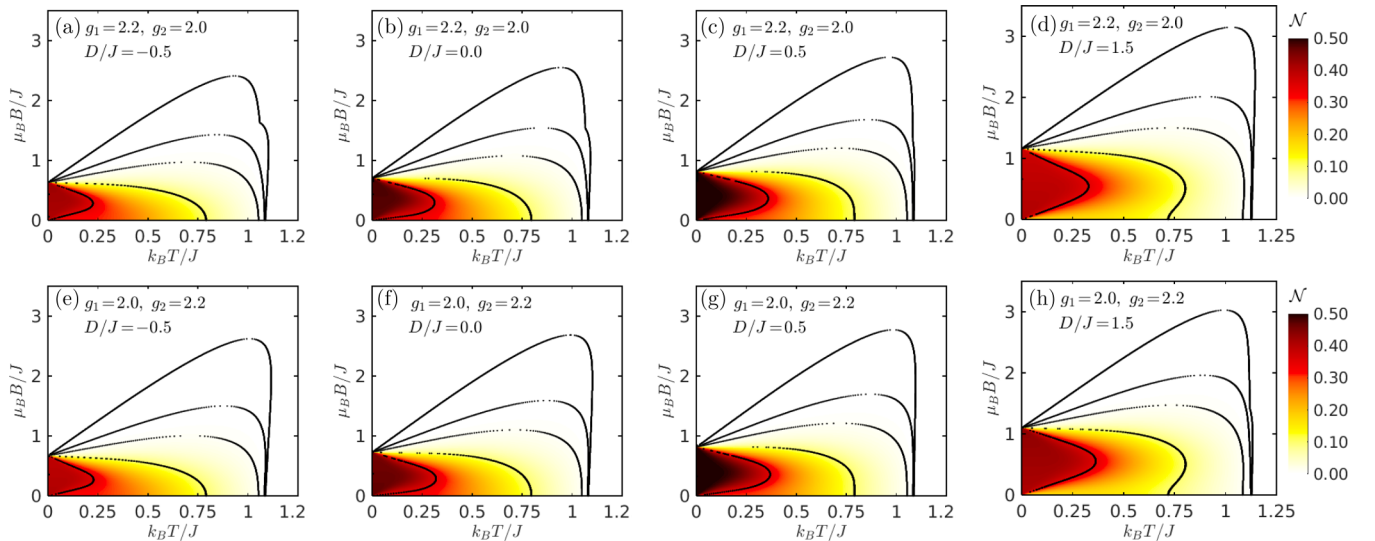

FIG. 7. Density plots of the negativity $\mathcal{N}$ in the $k_B T/J$-$\mu_B B/J$ plane for $\Delta = 1.0$, two different set of the Landé g factors $g_1 > g_2$ and $g_1 < g_2$ with the same relative difference $|g_1 - g_2| = 0.2$, and several values of the uniaxial single-ion anisotropy D/J. The black contour lines correspond to $\mathcal{N} = 0.35, 0.1, 0.01, 0.001,$ and 10^{-5} (from left to right).
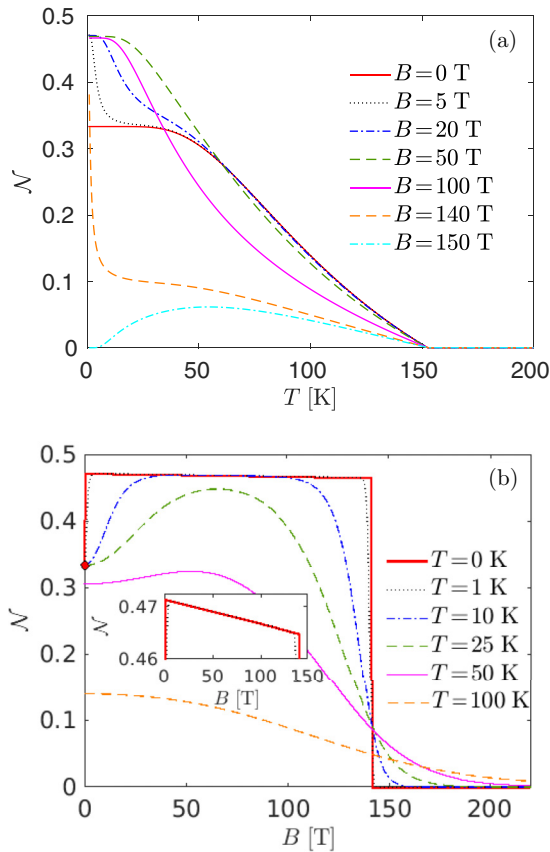
FIG. 8. (a) Temperature dependences of the negativity $\mathcal{N}$ conforming to the CuNi compound for several values of the magnetic field. (b) Magnetic-field dependences of the negativity $\mathcal{N}$ conforming to the CuNi compound for several values of temperature (the inset shows in an enhanced scale a quasiplateau region). All displayed dependences were obtained for the mixed spin-(1/2, 1) Heisenberg dimer with the isotropic exchange constant $J/k_B = 141$ K ($\Delta = 1$), a zero single-ion anisotropy ($D/k_B = 0$ K), and the gyromagnetic g factors $g_1 = 2.20$ and $g_2 = 2.29$ adapted according to Ref. [70].

FIG. 9. A density plot of the negativity $\mathcal{N}$ in the temperature-field plane conforming to the CuNi compound. The presented plot was obtained for the mixed spin-(1/2, 1) Heisenberg dimer with the isotropic exchange constant $J/k_B = 141$ K ($\Delta = 1$), a zero single-ion anisotropy ($D/k_B = 0$ K), and the gyromagnetic g factors $g_1 = 2.20$ and $g_2 = 2.29$ adapted according to Ref. [70]. Black contour lines correspond to the particular values $\mathcal{N} = 0.3$, 0.1, and 0.01 (from left to right).

then it rises to a local maximum, which is successively followed by a gradual reduction until it again disappears at an upper threshold temperature (see the curve for $B = 150$ T).

The isothermal dependence of the negativity on a magnetic field shown in Fig. 8(b) corroborates a transient strengthening of the thermal entanglement due to the external magnetic field. Owing to a difference of the gyromagnetic g factors $g_1 = 2.20$ and $g_2 = 2.29$ of Cu^{2+} and Ni^{2+} magnetic ions, the negativity exhibits at very low temperatures $T \lesssim 1$ K a quasilinear decrease (quasiplateau) [see the inset in Fig. 8(b)], which is quite analogous to a quasiplateau predicted for low-temperature magnetization curves of quantum Heisenberg spin systems with different g factors [71]. Moreover, the negativity starts at sufficiently low temperatures $T \lesssim 25$ K from the initial value $\mathcal{N} = 1/3$, then it gradually increases to its local maximum before it finally diminishes upon further increase of the magnetic field. It is noteworthy that the initial value of the negativity is suppressed and its local maximum becomes more flat at moderate temperatures (e.g., for $T = 50$ K), while the negativity monotonically decreases upon strengthening
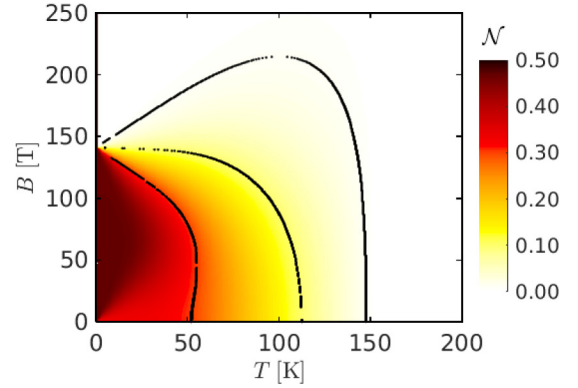
the external magnetic field at higher temperatures (e.g., for $T = 100$ K).

Finally, the density plot of the negativity in the temperature-field plane is depicted in Fig. 9 for the mixed spin-(1/2, 1) Heisenberg dimer with the isotropic exchange constant $J/k_B = 141$ K ($\Delta = 1$), the gyromagnetic g factors $g_1 = 2.20$ and $g_2 = 2.29$, which correspond according to Ref. [70] to the heterodinuclear complex CuNi. The displayed density plot can be alternatively viewed as a kind of "phase diagram," which circumscribes a parameter space with a nonzero thermal entanglement from a disentangled parameter region. Although a subtle thermal entanglement can be detected even under extremely high magnetic fields and temperatures, the indispensable thermal entanglement of sufficient intensity (say $\mathcal{N} \gtrsim 0.1$) is confined to the magnetic fields $B \lesssim 140$ T and temperatures $T \lesssim 115$ K that are comparable with the relevant exchange constant. While the bound set for the magnetic field considerably exceeds a reasonable range of magnetic fields for possible technological applications, the respective bound set for temperature apparently indicates the necessity search for heterodinuclear complexes quite analogous to the CuNi compound [70] which would, however, possess at least twice as large an exchange constant in order to make technological applications at room temperatures viable.

D. Experimental testing of theoretical results

It should be emphasized that the negativity of the mixed spin-(1/2, 1) Heisenberg dimer was theoretically calculated according to the definition (13) from the eigenvalues (18)–(21), which are expressed in terms of density-matrix elements explicitly quoted in Appendix A. It is quite obvious that the individual elements of the density matrix cannot be directly measured and, hence, it necessary to suggest an alternative way that theoretical results for the negativity of the heterodinuclear complex CuNi [70] could be experimentally verified.

First, it is worthwhile to remark that the density-matrix elements ρ_{ij}, and thus the negativity, can be directly connected to a few local observables calculated according to the formula $\langle \hat{O} \rangle = \text{Tr} \, \hat{O} \hat{\rho}$. It is easy to convince oneself that the five local expectation values $\langle \hat{S}^z \rangle$, $\langle \hat{\mu}^z \rangle$, $\langle (\hat{\mu}^z)^2 \rangle$, $\langle \hat{S}^z \hat{\mu}^z \rangle$, and $\langle \hat{S}^z (\hat{\mu}^z)^2 \rangle$ can be easily related to diagonal elements of the density matrix:

$$\langle \hat{S}^z \rangle = \text{Tr} \, \hat{\rho} \hat{S}^z = \tfrac{1}{2}(\rho_{11} + \rho_{22} + \rho_{33} - \rho_{44} - \rho_{55} - \rho_{66}),$$

$$\langle \hat{\mu}^z \rangle = \text{Tr} \, \hat{\rho} \hat{\mu}^z = \rho_{11} - \rho_{33} + \rho_{44} - \rho_{66},$$

$$\langle (\hat{\mu}^z)^2 \rangle = \text{Tr} \, \hat{\rho} (\hat{\mu}^z)^2 = \rho_{11} + \rho_{33} + \rho_{44} + \rho_{66}, \quad (29)$$

$$\langle \hat{S}^z \hat{\mu}^z \rangle = \text{Tr} \, \hat{\rho} \hat{S}^z \hat{\mu}^z = \tfrac{1}{2}(\rho_{11} - \rho_{33} - \rho_{44} + \rho_{66}),$$

$$\langle \hat{S}^z (\hat{\mu}^z)^2 \rangle = \text{Tr} \, \hat{\rho} \hat{S}^z (\hat{\mu}^z)^2 = \tfrac{1}{2}(\rho_{11} + \rho_{33} - \rho_{44} - \rho_{66}).$$

All diagonal elements of the density matrix ρ_{ii} can be consequently expressed in terms of the local expectation values $\langle \hat{S}^z \rangle$, $\langle \hat{\mu}^z \rangle$, $\langle (\hat{\mu}^z)^2 \rangle$, $\langle \hat{S}^z \hat{\mu}^z \rangle$, and $\langle \hat{S}^z (\hat{\mu}^z)^2 \rangle$ when additionally taking into account the trivial identity $\text{Tr} \, \hat{\rho} = \sum_{i=1}^{6} \rho_{ii} = 1$:

$$\rho_{11} = \tfrac{1}{4}[\langle (\hat{\mu}^z)^2 \rangle + 2\langle \hat{S}^z \hat{\mu}^z \rangle + 2\langle \hat{S}^z (\hat{\mu}^z)^2 \rangle + \langle \hat{\mu}^z \rangle], \quad (30)$$

$$\rho_{22} = \tfrac{1}{2}[1 - \langle (\hat{\mu}^z)^2 \rangle + 2\langle \hat{S}^z \rangle - 2\langle \hat{S}^z (\hat{\mu}^z)^2 \rangle], \quad (31)$$

$$\rho_{33} = \tfrac{1}{4}[\langle (\hat{\mu}^z)^2 \rangle - 2\langle \hat{S}^z \hat{\mu}^z \rangle + 2\langle \hat{S}^z (\hat{\mu}^z)^2 \rangle - \langle \hat{\mu}^z \rangle], \quad (32)$$

$$\rho_{44} = \tfrac{1}{4}[\langle (\hat{\mu}^z)^2 \rangle - 2\langle \hat{S}^z \hat{\mu}^z \rangle - 2\langle \hat{S}^z (\hat{\mu}^z)^2 \rangle + \langle \hat{\mu}^z \rangle], \quad (33)$$

$$\rho_{55} = \tfrac{1}{2}[1 - \langle (\hat{\mu}^z)^2 \rangle - 2\langle \hat{S}^z \rangle + 2\langle \hat{S}^z (\hat{\mu}^z)^2 \rangle], \quad (34)$$

$$\rho_{66} = \tfrac{1}{4}[\langle (\hat{\mu}^z)^2 \rangle + 2\langle \hat{S}^z \hat{\mu}^z \rangle - 2\langle \hat{S}^z (\hat{\mu}^z)^2 \rangle - \langle \hat{\mu}^z \rangle]. \quad (35)$$

Next, four nonzero off-diagonal elements of the density matrix $\rho_{24} = \rho_{42}$ and $\rho_{35} = \rho_{53}$ can be related to the local pair correlation function $\langle \hat{S}^x \hat{\mu}^x \rangle$ through the relation

$$\langle \hat{S}^x \hat{\mu}^x \rangle = \text{Tr} \, \hat{\rho} \hat{S}^x \hat{\mu}^x = \frac{1}{\sqrt{2}}(\rho_{24} + \rho_{35}), \quad (36)$$

which can be additionally supplemented with the inter-relation between two inequivalent off-diagonal elements,

$$\rho_{24} = \rho_{35} e^{\beta h_2} \sqrt{\frac{[J - 2D + 2(h_1 - h_2)]^2 + 8(J\Delta)^2}{[J - 2D - 2(h_1 - h_2)]^2 + 8(J\Delta)^2}}$$

$$\times \frac{\sinh\left(\frac{\beta}{4}\sqrt{[J - 2D - 2(h_1 - h_2)]^2 + 8(J\Delta)^2}\right)}{\sinh\left(\frac{\beta}{4}\sqrt{[J - 2D + 2(h_1 - h_2)]^2 + 8(J\Delta)^2}\right)}. \quad (37)$$

After straightforward, but tedious algebra, one may derive from Eqs. (36) and (37) the following formulas for nonzero off-diagonal elements of the density matrix:

$$\rho_{24} = \rho_{42} = \langle \hat{S}^x \hat{\mu}^x \rangle K_{24}, \quad (38)$$

$$\rho_{35} = \rho_{53} = \langle \hat{S}^x \hat{\mu}^x \rangle K_{35}, \quad (39)$$

which include the coefficients K_{24} and K_{35} explicitly given in Appendix B. In this way, we have successfully expressed all nonzero density-matrix elements determining the negativity through six local expectation values, $\langle \hat{S}^z \rangle$, $\langle \hat{\mu}^z \rangle$, $\langle (\hat{\mu}^z)^2 \rangle$, $\langle \hat{S}^z \hat{\mu}^z \rangle$, $\langle \hat{S}^z (\hat{\mu}^z)^2 \rangle$, and $\langle \hat{S}^x \hat{\mu}^x \rangle$. Although the aforementioned set of local observables is not directly accessible by means of standard magnetometry measurements, recent advances in inelastic neutron scattering experiments pave the way towards indirect determination of the local spin correlations from the relevant structure factors [72–76].

For the sake of completeness, we have listed in Appendix C an explicit form of expectation values for all local observables determining the density-matrix elements. The derived formulas suggest that the three local observables $\langle \hat{S}^z \rangle = \langle \hat{\mu}^z \rangle = \langle \hat{S}^z (\hat{\mu}^z)^2 \rangle = 0$ become zero in the absence of an external magnetic field, which basically simplifies determination of the negativity for this special case. Besides, the heterodinuclear complex CuNi does not exhibit, according to Ref. [70], either exchange or uniaxial single-ion anisotropy, which additionally implies the equality $\langle \hat{S}^z \hat{\mu}^z \rangle = \langle \hat{S}^x \hat{\mu}^x \rangle$ between two components of the pair correlation function due to the underlying SU(2) symmetry. Consequently, the negativity of the dimeric compound CuNi [70] can be determined in zero magnetic field solely from two independent local observables $\langle \hat{S}^z \hat{\mu}^z \rangle$ and $\langle (\hat{\mu}^z)^2 \rangle$, which can be alternatively obtained from easily accessible experimental data of zero-field susceptibility [19–24] and specific heat [25,26]. Unfortunately, the experimental data for the specific heat needed for a concurrent determination of two local observables $\langle \hat{S}^z \hat{\mu}^z \rangle$ and $\langle (\hat{\mu}^z)^2 \rangle$ are unavailable unlike the susceptibility data reported in Ref. [70], which currently precludes calculation of the negativity of the molecular complex CuNi from experimental data. However, it is our hope that the present theoretical study will stimulate future experimental testing of the thermal entanglement of the molecular compound CuNi either through inelastic neutron scattering or specific-heat measurements.

IV. CONCLUSION

In the present article we have exactly examined the negativity of a mixed spin-(1/2, 1) Heisenberg dimer, which quantifies the strength of the bipartite quantum and thermal entanglement at zero as well as nonzero temperatures within pure and mixed states of this simple quantum spin system. It has been evidenced that the negativity basically depends on intrinsic parameters such as exchange and uniaxial single-ion anisotropy in addition to extrinsic parameters such as temperature and magnetic field. The strongest quantum entanglement at zero temperature and zero magnetic field has been found for the particular case without uniaxial single-ion anisotropy and a perfectly isotropic coupling constant, while the negativity becomes completely independent of the exchange anisotropy for the specific strength of the uniaxial single-ion anisotropy $D/J = 1/2$. In the presence of an external magnetic field the situation becomes much more intricate, because the negativity depends on gyromagnetic g factors in addition to the exchange and uniaxial single-ion anisotropy, magnetic field, and temperature. It turns out that the particular case with equal Landé g factors exhibits the maximal quantum entanglement whenever the uniaxial single-ion anisotropy acquires the value $D/J = 1/2$.

In contrast to general expectations, the rising magnetic field remarkably reinforces the bipartite quantum entanglement due to the Zeeman splitting of energy levels, which lifts a twofold degeneracy of the quantum ferrimagnetic ground

state. The maximal quantum entanglement is thus reached within a quantum ferrimagnetic phase at sufficiently low but nonzero magnetic fields under the assumption that the gyromagnetic g factors are equal and the uniaxial single-ion anisotropy is half of the exchange constant $D/J = 1/2$. The strength of the bipartite quantum entanglement for the particular case with unequal gyromagnetic g factors shows a quasilinear dependence on the external magnetic field, which is quite reminiscent of a quasiplateau phenomenon reported previously for low-temperature magnetization curves of quantum spin systems being composed of entities with unequal gyromagnetic g factors [71]. It should be pointed out that all aforementioned generic trends are preserved for the bipartite thermal entanglement within the mixed states emergent at finite temperatures.

The heterodinuclear complex CuNi, as a prominent experimental representative of the mixed spin-(1/2, 1) Heisenberg dimer, afforded a useful playground for an investigation of the bipartite thermal entanglement in a real-world system. It appears worthwhile to remark that the dimeric complex CuNi

remains strongly entangled up to relatively high temperatures (about 115 K) and high magnetic fields (about 140 T) that are comparable with the relevant exchange constant. From this point of view, the magnitude of the coupling constant in the heterodinuclear complex CuNi is inadequate for prospective technological applications of this solid-state material in quantum computing and quantum information processing at room temperature. An enhancement of the coupling constant through the targeted design of a related heterodinuclear coordination compound of the type CuNi thus represents a challenging task for materials scientists.

APPENDIX A

The explicit forms of nonzero elements ρ_{ij} of the density matrix given by Eq. (16) are

$$\rho_{11} = \frac{1}{Z} e^{-\frac{\beta}{2}[J+2D-(h_1+2h_2)]}, \tag{A1}$$

$$\rho_{22} = \frac{1}{Z} e^{\frac{\beta}{4}(J-2D+2h_2)} \left[\cosh\left(\frac{\beta}{4}\sqrt{[J-2D-2(h_1-h_2)]^2 + 8(J\Delta)^2} \right) - \frac{J-2D-2(h_1-h_2)}{\sqrt{[J-2D-2(h_1-h_2)]^2 + 8(J\Delta)^2}} \right.$$
$$\left. \times \sinh\left(\frac{\beta}{4}\sqrt{[J-2D-2(h_1-h_2)]^2 + 8(J\Delta)^2} \right) \right], \tag{A2}$$

$$\rho_{33} = \frac{1}{Z} e^{\frac{\beta}{4}(J-2D-2h_2)} \left[\cosh\left(\frac{\beta}{4}\sqrt{[J-2D+2(h_1-h_2)]^2 + 8(J\Delta)^2} \right) + \frac{J-2D+2(h_1-h_2)}{\sqrt{[J-2D+2(h_1-h_2)]^2 + 8(J\Delta)^2}} \right.$$
$$\left. \times \sinh\left(\frac{\beta}{4}\sqrt{[J-2D+2(h_1-h_2)]^2 + 8(J\Delta)^2} \right) \right], \tag{A3}$$

$$\rho_{44} = \frac{1}{Z} e^{\frac{\beta}{4}(J-2D+2h_2)} \left[\cosh\left(\frac{\beta}{4}\sqrt{[J-2D-2(h_1-h_2)]^2 + 8(J\Delta)^2} \right) + \frac{J-2D-2(h_1-h_2)}{\sqrt{[J-2D-2(h_1-h_2)]^2 + 8(J\Delta)^2}} \right.$$
$$\left. \times \sinh\left(\frac{\beta}{4}\sqrt{[J-2D-2(h_1-h_2)]^2 + 8(J\Delta)^2} \right) \right], \tag{A4}$$

$$\rho_{55} = \frac{1}{Z} e^{\frac{\beta}{4}(J-2D-2h_2)} \left[\cosh\left(\frac{\beta}{4}\sqrt{[J-2D+2(h_1-h_2)]^2 + 8(J\Delta)^2} \right) - \frac{J-2D+2(h_1-h_2)}{\sqrt{[J-2D+2(h_1-h_2)]^2 + 8(J\Delta)^2}} \right.$$
$$\left. \times \sinh\left(\frac{\beta}{4}\sqrt{[J-2D+2(h_1-h_2)]^2 + 8(J\Delta)^2} \right) \right], \tag{A5}$$

$$\rho_{66} = \frac{1}{Z} e^{-\frac{\beta}{2}[J+2D+(h_1+2h_2)]}, \tag{A6}$$

$$\rho_{24} = \rho_{42} = -\frac{\sqrt{8} J\Delta e^{\frac{\beta}{4}(J-2D+2h_2)}}{Z\sqrt{[J-2D-2(h_1-h_2)]^2 + 8(J\Delta)^2}} \sinh\left(\frac{\beta}{4}\sqrt{[J-2D-2(h_1-h_2)]^2 + 8(J\Delta)^2} \right), \tag{A7}$$

$$\rho_{35} = \rho_{53} = -\frac{\sqrt{8} J\Delta e^{\frac{\beta}{4}(J-2D-2h_2)}}{Z\sqrt{[J-2D+2(h_1-h_2)]^2 + 8(J\Delta)^2}} \sinh\left(\frac{\beta}{4}\sqrt{[J-2D+2(h_1-h_2)]^2 + 8(J\Delta)^2} \right). \tag{A8}$$

APPENDIX B

The explicit forms of the coefficients K_{24} and K_{35} entering into Eqs. (38) and (39) are

$$
K_{24} = \sqrt{2} \frac{e^{\frac{\beta}{2}h_2} \sinh\left(\frac{\beta}{4}\sqrt{[J - 2D - 2(h_1 - h_2)]^2 + 8(J\Delta)^2}\right)}{\sqrt{[J - 2D - 2(h_1 - h_2)]^2 + 8(J\Delta)^2}}
$$
$$
\times \left(\frac{e^{\frac{\beta}{2}h_2} \sinh\left(\frac{\beta}{4}\sqrt{[J - 2D - 2(h_1 - h_2)]^2 + 8(J\Delta)^2}\right)}{\sqrt{[J - 2D - 2(h_1 - h_2)]^2 + 8(J\Delta)^2}} + \frac{e^{-\frac{\beta}{2}h_2} \sinh\left(\frac{\beta}{4}\sqrt{[J - 2D + 2(h_1 - h_2)]^2 + 8(J\Delta)^2}\right)}{\sqrt{[J - 2D + 2(h_1 - h_2)]^2 + 8(J\Delta)^2}} \right)^{-1}, \quad \text{(B1)}
$$
$$
K_{35} = \sqrt{2} \frac{e^{-\frac{\beta}{2}h_2} \sinh\left(\frac{\beta}{4}\sqrt{[J - 2D + 2(h_1 - h_2)]^2 + 8(J\Delta)^2}\right)}{\sqrt{[J - 2D + 2(h_1 - h_2)]^2 + 8(J\Delta)^2}}
$$
$$
\times \left(\frac{e^{\frac{\beta}{2}h_2} \sinh\left(\frac{\beta}{4}\sqrt{[J - 2D - 2(h_1 - h_2)]^2 + 8(J\Delta)^2}\right)}{\sqrt{[J - 2D - 2(h_1 - h_2)]^2 + 8(J\Delta)^2}} + \frac{e^{-\frac{\beta}{2}h_2} \sinh\left(\frac{\beta}{4}\sqrt{[J - 2D + 2(h_1 - h_2)]^2 + 8(J\Delta)^2}\right)}{\sqrt{[J - 2D + 2(h_1 - h_2)]^2 + 8(J\Delta)^2}} \right)^{-1}. \quad \text{(B2)}
$$

APPENDIX C

The explicit forms of the expectation values, which may be used for calculation of all density matrix elements according to Eqs. (30)–(35) and (38)–(39), are

$$
\langle \hat{S}^z \rangle = \frac{1}{Z} \frac{\partial Z}{\partial \beta h_1} = \frac{1}{Z} \Bigg\{ e^{-\frac{\beta}{2}(J+2D)} \sinh\left(\frac{\beta}{2}(h_1 + 2h_2)\right)
$$
$$
- e^{\frac{\beta}{4}(J-2D)} \Bigg[\frac{e^{\frac{\beta}{2}h_2}[J - 2D - 2(h_1 - h_2)]}{\sqrt{[J - 2D - 2(h_1 - h_2)]^2 + 8(J\Delta)^2}} \sinh\left(\frac{\beta}{4}\sqrt{[J - 2D - 2(h_1 - h_2)]^2 + 8(J\Delta)^2}\right)
$$
$$
- \frac{e^{-\frac{\beta}{2}h_2}[J - 2D + 2(h_1 - h_2)]}{\sqrt{[J - 2D + 2(h_1 - h_2)]^2 + 8(J\Delta)^2}} \sinh\left(\frac{\beta}{4}\sqrt{[J - 2D + 2(h_1 - h_2)]^2 + 8(J\Delta)^2}\right) \Bigg] \Bigg\}, \quad \text{(C1)}
$$
$$
\langle \hat{\mu}^z \rangle = \frac{1}{Z} \frac{\partial Z}{\partial \beta h_2} = \frac{1}{Z} \Bigg\{ 2e^{-\frac{\beta}{2}(J+2D)} \sinh\left(\frac{\beta}{2}(h_1 + 2h_2)\right)
$$
$$
+ e^{\frac{\beta}{4}(J-2D)} \Bigg\{ e^{\frac{\beta}{2}h_2} \Bigg[\cosh\left(\frac{\beta}{4}\sqrt{[J - 2D - 2(h_1 - h_2)]^2 + 8(J\Delta)^2}\right) + \frac{J - 2D - 2(h_1 - h_2)}{\sqrt{[J - 2D - 2(h_1 - h_2)]^2 + 8(J\Delta)^2}}
$$
$$
\times \sinh\left(\frac{\beta}{4}\sqrt{[J - 2D - 2(h_1 - h_2)]^2 + 8(J\Delta)^2}\right) \Bigg] - e^{-\frac{\beta}{2}h_2} \Bigg[\cosh\left(\frac{\beta}{4}\sqrt{[J - 2D + 2(h_1 - h_2)]^2 + 8(J\Delta)^2}\right)
$$
$$
+ \frac{J - 2D + 2(h_1 - h_2)}{\sqrt{[J - 2D + 2(h_1 - h_2)]^2 + 8(J\Delta)^2}} \sinh\left(\frac{\beta}{4}\sqrt{[J - 2D + 2(h_1 - h_2)]^2 + 8(J\Delta)^2}\right) \Bigg] \Bigg\} \Bigg\}, \quad \text{(C2)}
$$
$$
\langle (\hat{\mu}^z)^2 \rangle = -\frac{1}{Z} \frac{\partial Z}{\partial \beta D} = \frac{1}{Z} \Bigg\{ 2e^{-\frac{\beta}{2}(J+2D)} \cosh\left(\frac{\beta}{2}(h_1 + 2h_2)\right)
$$
$$
+ e^{\frac{\beta}{4}(J-2D)} \Bigg\{ e^{\frac{\beta}{2}h_2} \Bigg[\cosh\left(\frac{\beta}{4}\sqrt{[J - 2D - 2(h_1 - h_2)]^2 + 8(J\Delta)^2}\right) + \frac{J - 2D - 2(h_1 - h_2)}{\sqrt{[J - 2D - 2(h_1 - h_2)]^2 + 8(J\Delta)^2}}
$$
$$
\times \sinh\left(\frac{\beta}{4}\sqrt{[J - 2D - 2(h_1 - h_2)]^2 + 8(J\Delta)^2}\right) \Bigg] + e^{-\frac{\beta}{2}h_2} \Bigg[\cosh\left(\frac{\beta}{4}\sqrt{[J - 2D + 2(h_1 - h_2)]^2 + 8(J\Delta)^2}\right)
$$
$$
+ \frac{J - 2D + 2(h_1 - h_2)}{\sqrt{[J - 2D + 2(h_1 - h_2)]^2 + 8(J\Delta)^2}} \sinh\left(\frac{\beta}{4}\sqrt{[J - 2D + 2(h_1 - h_2)]^2 + 8(J\Delta)^2}\right) \Bigg] \Bigg\} \Bigg\}, \quad \text{(C3)}
$$
$$
\langle \hat{S}^x \hat{\mu}^x \rangle = -\frac{1}{2Z} \frac{\partial Z}{\partial \beta \Delta} = \frac{-2J\Delta}{Z} e^{\frac{\beta}{4}(J-2D)} \Bigg[\frac{e^{\frac{\beta}{2}h_2} \sinh\left(\frac{\beta}{4}\sqrt{[J - 2D - 2(h_1 - h_2)]^2 + 8(J\Delta)^2}\right)}{\sqrt{[J - 2D - 2(h_1 - h_2)]^2 + 8(J\Delta)^2}}
$$
$$
+ \frac{e^{-\frac{\beta}{2}h_2} \sinh\left(\frac{\beta}{4}\sqrt{[J - 2D + 2(h_1 - h_2)]^2 + 8(J\Delta)^2}\right)}{\sqrt{[J - 2D + 2(h_1 - h_2)]^2 + 8(J\Delta)^2}} \Bigg], \quad \text{(C4)}
$$

$$
\langle \hat{S}^z \hat{\mu}^z \rangle = -\frac{1}{Z} \frac{\partial Z}{\partial \beta J} = \frac{1}{Z} \left\{ e^{-\frac{\beta}{2}(J+2D)} \cosh\left(\frac{\beta}{2}(h_1 + 2h_2)\right) \right.
$$

$$
- \frac{1}{2} e^{\frac{\beta}{4}(J-2D)} \left\{ e^{\frac{\beta}{2}h_2} \left[\cosh\left(\frac{\beta}{4}\sqrt{[J-2D-2(h_1-h_2)]^2 + 8(J\Delta)^2}\right) + \frac{J-2D-2(h_1-h_2)}{\sqrt{[J-2D-2(h_1-h_2)]^2 + 8(J\Delta)^2}} \right.\right.
$$

$$
\times \left. \sinh\left(\frac{\beta}{4}\sqrt{[J-2D-2(h_1-h_2)]^2 + 8(J\Delta)^2}\right) \right] + e^{-\frac{\beta}{2}h_2}\left[\cosh\left(\frac{\beta}{4}\sqrt{[J-2D+2(h_1-h_2)]^2 + 8(J\Delta)^2}\right) \right.
$$

$$
\left.\left.\left. + \frac{J-2D+2(h_1-h_2)}{\sqrt{[J-2D+2(h_1-h_2)]^2 + 8(J\Delta)^2}} \sinh\left(\frac{\beta}{4}\sqrt{[J-2D+2(h_1-h_2)]^2 + 8(J\Delta)^2}\right) \right] \right\}\right\}, \tag{C5}
$$

$$
\langle \hat{S}^z (\hat{\mu}^z)^2 \rangle = -\frac{\langle \hat{\mu}^z \rangle}{2} + \frac{2e^{-\frac{\beta}{2}(J+2D)}}{Z} \sinh\left(\frac{\beta}{2}(h_1 + 2h_2)\right). \tag{C6}
$$

[1] L. J. de Jongh and A. R. Miedema, Adv. Phys. **23**, 1 (1974).

[2] R. L. Carlin, *Magnetochemistry* (Springer, Berlin, 1986).

[3] O. Kahn, *Molecular Magnetism* (Wiley, New York, 1993).

[4] B. Sieklucka and D. Pinkowicz, *Molecular Magnetic Materials* (Wiley-VCH, Weinheim, 2017).

[5] M. N. Leuenberger and D. Loss, Nature (London) **410**, 789 (2001).

[6] L. K. Grover, Phys. Rev. Lett. **79**, 4709 (1997).

[7] L. Thomas, F. Lionti, R. Ballou, B. Barbara, D. Gatteschi, and R. Sessoli, Nature (London) **383**, 145 (1996).

[8] C. Sangregorio, T. Ohm, C. Paulsen, R. Sessoli, and D. Gatteschi, Phys. Rev. Lett. **78**, 4645 (1997).

[9] D. Gatteschi, R. Sessoli, and J. Villain, *Molecular Nanomagnets* (Oxford University Press, Oxford, 2006).

[10] P. Shor, in *Proceedings of the 35th Annual Symposium on Foundations of Computer Science*, edited by S. Goldwasser (IEEE Computer Society, Los Alamitos, CA, 1994), pp. 124–134.

[11] L. Amico, R. Fazio, A. Osterloh, and V. Vedral, Rev. Mod. Phys. **80**, 517 (2008).

[12] M. C. Arnesen, S. Bose, and V. Vedral, Phys. Rev. Lett. **87**, 017901 (2001).

[13] A. Peres, Phys. Rev. Lett. **77**, 1413 (1996).

[14] M. Horodecki, P. Horodecki, and R. Horodecki, Phys. Lett. A **223**, 1 (1996).

[15] G. Vidal and R. F. Werner, Phys. Rev. A **65**, 032314 (2002).

[16] W. K. Wootters, Phys. Rev. Lett. **80**, 2245 (1998).

[17] X. Wang and P. Zanardi, Phys. Lett. A **301**, 1 (2002).

[18] S. M. Aldoshin, E. B. Feldman, and M. A. Yurishchev, J. Exp. Theor. Phys. **107**, 804 (2008).

[19] A. M. Souza, M. S. Reis, D. O. Soares-Pinto, I. S. Oliveira, and R. S. Sarthour, Phys. Rev. B **77**, 104402 (2008).

[20] C. Cruz, D. O. Soares-Pinto, P. Brandao, A. M. dos Santos, and M. S. Reis, Europhys. Lett. **113**, 40004 (2016).

[21] D. O. Soares-Pinto, A. M. Souza, R. S. Sarthour, I. S. Oliveira, M. S. Reis, P. Brandao, J. Rocha, and A. M. dos Santos, Europhys. Lett. **87**, 40008 (2009).

[22] M. S. Reis, S. Soriano, A. M. dos Santos, B. C. Sales, D. O. Soares-Pinto, and P. Brandao, Europhys. Lett. **100**, 50001 (2012).

[23] T. Chakraborty, T. K. Sen, H. Singh, D. Das, S. K. Mandal, and C. Mitra, J. Appl. Phys. **114**, 144904 (2013).

[24] C. Cruz and M. F. Anka, Europhys. Lett. **130**, 30006 (2020).

[25] T. Chakraborty, H. Singh, S. Singh, R. K. Gopal, and C. Mitra, J. Phys.: Condens. Matter **25**, 425601 (2013).

[26] T. Chakraborty, H. Singh, and C. Mitra, J. Appl. Phys. **115**, 034909 (2014).

[27] Y. Yeo, Phys. Rev. A **66**, 062312 (2002).

[28] M. Rojas, S. M. de Souza, and O. Rojas, Ann. Phys. (NY) **377**, 506 (2017).

[29] M. Freitas, C. Filgueiras, and M. Rojas, Ann. Phys. (NY) **531**, 1900261 (2019).

[30] Y.-D. Zheng, Z. Mao, and B. Zhou, Chin. Phys. B **28**, 120307 (2019).

[31] X. Wang, Phys. Lett. A **281**, 101 (2001).

[32] A. Abliz, H. J. Gao, X. C. Xie, Y. S. Wu, and W. M. Liu, Phys. Rev. A **74**, 052105 (2006).

[33] H. Fu, A. I. Solomon, and X. Wang, J. Phys. A: Math. Gen. **35**, 4293 (2002).

[34] I. Bose and A. Tribedi, Phys. Rev. A **72**, 022314 (2005).

[35] M. Cao and S. Zhu, Phys. Rev. A **71**, 034311 (2005).

[36] K. Karl'ová and J. Strečka, Acta Phys. Pol. A **137**, 595 (2020).

[37] X. Wang, Phys. Rev. A **66**, 044305 (2002).

[38] Y. Chen, P. Zanardi, Z. D. Wang, and F. C. Zhang, New J. Phys. **8**, 97 (2006).

[39] A. Tribedi and I. Bose, Phys. Rev. A **79**, 012331 (2009).

[40] O. Rojas, J. Strečka, and S. M. de Souza, Solid State Commun. **246**, 68 (2016).

[41] J. Strečka, R. C. Alécio, M. L. Lyra, and O. Rojas, J. Magn. Magn. Mater. **409**, 124 (2016).

[42] R. C. Alécio, M. L. Lyra, and J. Strečka, J. Magn. Magn. Mater. **417**, 294 (2016).

[43] O. Rojas, J. Strečka, and M. L. Lyra, Phys. Lett. A **377**, 920 (2013).

[44] J. Strečka, O. Rojas, T. Verkholyak, and M. L. Lyra, Phys. Rev. E **89**, 022143 (2014).

[45] J. Strečka and J. Pavličko, Acta Phys. Pol. A **132**, 167 (2017).

[46] J. Torrico, M. Rojas, S. M. de Souza, O. Rojas, and N. S. Ananikian, Europhys. Lett. **108**, 50007 (2014).

[47] J. Qiao and B. Zhou, Chin. Phys. B **24**, 110306 (2015).

[48] O. Rojas, M. Rojas, S. M. de Souza, J. Torrico, J. Strečka, and M. L. Lyra, Physica A **486**, 367 (2017).

[49] Y. Zheng, Z. Mao, and B. Zhou, Chin. Phys. B **27**, 090306 (2018).

[50] I. M. Carvalho, J. Torrico, S. M. de Souza, M. Rojas, and O. Rojas, J. Magn. Magn. Mater. **465**, 323 (2018).

[51] I. M. Carvalho, O. Rojas, S. M. de Souza, and M. Rojas, Quantum Inf. Process. **18**, 134 (2019).

[52] K. Karl'ová, J. Strečka, and M. L. Lyra, Phys. Rev. B **97**, 104407 (2018).

[53] F. Souza, M. L. Lyra, J. Strečka, and M. S. S. Pereira, J. Magn. Magn. Mater. **471**, 423 (2019).

[54] K. Karl'ová, J. Strečka, and M. L. Lyra, Phys. Rev. E **100**, 042127 (2019).

[55] X. Wang and Z. D. Wang, Phys. Rev. A **73**, 064302 (2006).

[56] H. Huang, X. Wang, Z. Sun, and G. Yang, Physica A **387**, 2736 (2006).

[57] Z. Sun, X. G. Wang, A. Z. Hu, and Y.-Q. Li, Physica A **370**, 483 (2006).

[58] Z. Sun, X.-M. Lu, H.-N. Xiong, and J. Ma, New J. Phys. **11**, 113005 (2009).

[59] Z. Sun, X. Wang, and H.-N. Xiong, Physica A **388**, 1337 (2009).

[60] E. Solano-Carrilo, R. Franco, and J. Silva-Valencia, Physica A **390**, 2208 (2011).

[61] E. Solano-Carrilo, R. Franco, and J. Silva-Valencia, Phys. Lett. A **375**, 1032 (2011).

[62] J.-L. Guo, X.-L. Huang, and H.-S. Song, Phys. Scr. **76**, 327 (2007).

[63] G.-H. Yang and L. Zhou, Phys. Scr. **78**, 025703 (2008).

[64] F. Wang, H. Jia, H. Zhang, X. Zhang, and S. Chang, Sci. China Ser. G **52**, 1919 (2009).

[65] G.-Q. Zhu, Cent. Eur. J. Phys. **7**, 135 (2009).

[66] S. Xu, X. Song, and L. Ye, Quantum Inf. Process. **13**, 1013 (2014).

[67] F. Wang, L.-P. Fu, and K.-T. Guo, Commun. Theor. Phys. **50**, 341 (2008).

[68] S. D. Han, T. Tüfekçi, T. P. Spiller, and E. Aydiner, Int. J. Theor. Phys. **56**, 1474 (2017).

[69] V. S. Abgaryan, N. S. Ananikian, L. N. Ananikyan, and V. Hovhannisyan, Solid State Commun. **203**, 5 (2015).

[70] M. Hagiwara, Y. Narumi, K. Minami, K. Tatani, and K. Kindo, J. Phys. Soc. Jpn. **68**, 2214 (1999).

[71] V. Ohanyan, O. Rojas, J. Strečka, and S. Bellucci, Phys. Rev. B **92**, 214423 (2015).

[72] S. W. Lovesey, *The Theory of Neutron Scattering from Condensed Matter*, Vol. 2 (Clarendon Press, Oxford, 1984).

[73] J. T. Haraldsen, T. Barnes, and J. L. Musfeldt, Phys. Rev. B **71**, 064403 (2005).

[74] C. Cruz, Int. J. Quantum Inf. **15**, 1750031 (2017).

[75] S. E. Nagler and D. A. Tennant, J. Phys.: Condens. Matter **32**, 374004 (2020).

[76] Y. Su, S. Wang, and C. Zhang, arXiv:2009.01680.